Influence of Nonuniform Geometry on Nanoindentation of Viral Capsids

Melissa M. Gibbons* and William S. Klug*†

*Department of Mechanical and Aerospace Engineering, †California NanoSystems Institute, and Program in Biomedical Engineering, University of California, Los Angeles, California

ABSTRACT A series of recent nanoindentation experiments on the protein shells (capsids) of viruses has established atomic force microscopy (AFM) as a useful framework for probing the mechanics of large protein assemblies. Specifically these experiments provide an opportunity to study the coupling of the global assembly response to local conformational changes. AFM experiments on cowpea chlorotic mottle virus, known to undergo a pH-controlled swelling conformational change, have revealed a pH-dependent mechanical response. Previous theoretical studies have shown that homogeneous changes in shell geometry can play a significant role in the mechanical response. This article develops a method for accurately capturing the heterogeneous geometry of a viral capsid and explores its effect on mechanical response with a nonlinear continuum elasticity model. Models of both native and swollen cowpea chlorotic mottle virus capsids are generated from x-ray crystal structures, and are used in finite element simulations of AFM indentation along two-, three-, and fivefold icosahedral symmetry orientations. The force response of the swollen capsid model is observed to be softer by roughly a factor of two, significantly more nonlinear, and more orientation-dependent than that of a native capsid with equivalent elastic moduli, demonstrating that capsid geometric heterogeneity can have significant effects on the global structural response.

INTRODUCTION

Because of the extensive information that is available about their reproducible structural organization and structural response to environmental stimuli, protein shells of viruses, or capsids, provide an ideal testing ground for the study of the mechanical material properties of two-dimensional protein assemblies. Understanding of the physical properties of viruses has been important in their use in nanotechnology applications (1,2), in design of new virus-based materials (3,4), and for a deeper understanding of the relationship between mechanics and infectivity (5). In the last few years, atomic force microscopy (AFM) has been established as an experimental means of probing viral mechanics by measuring the force response of individual capsids during indentation between a glass substrate and an approximately round AFM tip. Most of the recent flurry of research activity on capsid nanoindentation has been summarized in two recent review articles (6,7).

Cowpea chlorotic mottle virus (CCMV), a roughly spherical plant virus, has been the focus of two recent nanoindentation studies (8,9). CCMV provides a model structure for studying the link between capsid chemistry and mechanical response because it self-assembles in vitro over a range of buffer conditions to form protein sheets with a variety of morphologies (10). The CCMV capsid, which protects a single-stranded RNA genome, is assembled from 180 identical protein subunits with 190 residues each arranged into a truncated icosahedron with a triangulation number $T = 3$, according to the Caspar-Klug classification scheme for icosahedral viruses (11). Like all icosahedral viruses, CCMV possesses the structural symmetries of an icosahedron, identified by two-, three-, and fivefold symmetry axes. The 180 CCMV subunits are arranged into 12 pentamers with fivefold symmetry and 20 hexamers with threefold (or quasi-sixfold) symmetry, while the twofold symmetry sites are found between adjacent hexamers. Additionally, quasi-threefold symmetry sites can be found at junctions where two hexamers contact a pentamer.

The fully packaged CCMV capsid exists in two distinct structural states (12–14). The native structure of the wild-type CCMV capsid, which is stable at pH 5 either with or without the genome, has an average diameter of ~28 nm and an average inner diameter of ~21 nm. As the pH is raised to ~7 at low ionic strength, a reversible swelling transition occurs in which the average radius increases by ~10% for the full capsid, whereas the empty capsid becomes unstable and dissociates. Although the empty capsid of wild-type CCMV is unstable at pH 7, a mutant (salt-stable) has been obtained, which remains stable as a swollen capsid even at high pH and ionic strength (15). The geometry of the native and swollen forms of the wild-type CCMV capsid are described to high resolution by x-ray crystal and cryo-EM structures (13). The first 26 residues are not visible in the cryo-EM map (13), and are therefore disordered, and should not be expected to function in any load-bearing capacity. It is known that the disordered residues play a role in interactions with the RNA (13). These structures indicate that the swelling of the capsid is in response to electrostatic repulsion of negatively charged acidic residues at the center of the quasi-threefold site, which causes a pore to open between the three subunits. The hexamers and pentamers do not deform greatly, but rather move relative to one another as the capsid expands. Functionally, the appearance of pores in the swollen state of CCMV is

Submitted April 25, 2008, and accepted for publication June 27, 2008.

Address reprint requests to William S. Klug, Tel.: 310-794-7347; E-mail: klug@ucla.edu.

Editor: Klaus Schulten.

0006-3495/08/10/3640/10 $2.00

doi: 10.1529/biophysj.108.136176

believed to play a role in the disassembly process that releases the genome into the host cell.

As shown in recent nanoindentation experiments, the influence of increasing pH is manifest in changes to the mechanical response of CCMV even before the structure of the capsid begins to change. Experiments performed on the empty wild-type capsid in its native state, at pH 5, reveal a structure that is relatively stiff but prone to breakage (8,9). Experiments performed on the empty capsid at pH 6 reveal a capsid that is approximately three times softer and remains elastic even when indented by an amount equal to its inner diameter, with no observed failure (9). The capsid at pH 6 had no measurable difference in height profile from the native, and therefore did not appear to be physically swollen, seeming to rule out any interpretation of the mechanical change as being linked to changes in geometry. Accordingly Klug et al. (9) accounted for changes in response by showing how treatment of the swelling as a pH-excited soft elastic mode within a Ginzburg-Landau framework leads to a renormalization of the effective Young's modulus and Föppel-von Kármán number. In this way, variation of the global constitutive parameters of the continuum shell model represents a coarse-graining of the pH-affected molecular interactions at the local scale of individual capsid proteins.

Although homogenized continuum elastic models like that in Klug et al. (9) and elsewhere (5,8,16–20) provide an explanation of capsid indentation mechanics consistent with experiments, the degree to which heterogeneity in these protein assemblies affects their global mechanical response is still unclear. In the case of the swelling transition of CCMV, local changes are obtained in both the structure and the interactions at the quasi-threefold sites, providing an opportunity to assess the mechanical effects of geometric and constitutive heterogeneities.

A number of previous modeling studies have suggested that the global mechanical response of capsids (6) and individual proteins (21) is influenced more by shape or geometric structure than by the subtleties of atomic interactions. Motivated by these findings, this article presents a model that addresses the effects of local, nonuniform geometric structure on the global capsid response, while still utilizing the framework of three-dimensional nonlinear continuum elasticity. Using structural data that accurately capture the nonuniform topography of both the native and swollen forms of the CCMV capsid, we present a systematic methodology of creating three-dimensional finite element meshes adhering to the macromolecular structure. This new model allows for the assessment of the effect of the geometric heterogeneity on softening between the native and swollen states. It is found that the protein rearrangements from the native to the swollen structure lead to measurable geometric softening, enhanced nonlinear character of the force-indentation response, and new local deformation modes. Based on the model we make two predictions, which should be experimentally testable: 1), that the swollen, pH 7 CCMV capsid should be at least twice as soft as the unswollen capsid at pH 6; and 2), that the force-indentation response of the swollen capsid should be more nonlinear and noticeably sensitive to the orientation of indentation relative to its symmetry axes.

METHODS

Smooth surface representations of macromolecules are commonly used for visualization purposes, and are featured in standard software packages such as Chimera (22) and VMD (23). Recently, methods have been developed to construct volumetric finite element meshes of macromolecules (24–26) based on smooth molecular surfaces. Here we use similar techniques to create coarse-grained three-dimensional continuum models that adhere to the geometric details of capsid structures determined by the methods of structural biology. In this article, we create models using atomic-level structural data from x-ray crystallography, but a similar meshing methodology has been developed for structural data in the form of electron density maps. A more in-depth study of the meshing approach along with a gallery of meshed viral capsids and nanoindentation simulations are presented elsewhere (M. Gibbons and W. Klug, unpublished). A synopsis of the two-step approach for constructing models is provided in the next section: first, molecular surfaces of the capsid are constructed from a low-resolution density map of the structure; and second, the region spanning the interior between molecular surfaces is tessellated with tetrahedra. The resulting tetrahedral mesh represents a discretization of a three-dimensional bulk elastic body modeling the capsid shell, which forms the structural input for finite element analysis of indentation as described in Nanoindentation Simulations.

Nonuniform capsid topography

The starting point for the generation of three-dimensional models is the acquisition of the atomic structure of the viral capsid of interest. Atomic coordinates for many proteins, viral capsids included, are available from the Protein Data Bank (28) and the Viper Data Bank (29). A mass density field that replaces the point mass at each atomic position is mathematically constructed with a truncated Gaussian density distribution. The densities of each atom are superposed, yielding a global density field that can be evaluated at any point, $\boldsymbol{r}$:

$$\rho(\boldsymbol{r}) = \sum_{i=1}^{\#\text{atoms}} \rho_i(\boldsymbol{r})$$
$$\rho_i(\boldsymbol{r}) = \begin{cases} \rho_0 e^{(-3|r-r_i|^2/2\sigma^2)}, & \text{if } |\boldsymbol{r}-\boldsymbol{r}_i| < r_{\max} \\ 0\ , & \text{otherwise.} \end{cases} \quad (1)$$

There are three parameters to be set in the density function: the amplitude, ρ_0, which is arbitrarily set to be 1.0 for each atom; the standard deviation, σ, which determines the width of the Gaussian and therefore the structural resolution of the surface; and the cutoff distance termed $r_{\max}$, beyond which the density value is considered zero. Here the cutoff distance is calculated as three times the standard deviation. Low values of the standard deviation keep the distance of influence around each atom small, increasing the level of detail of the density field. Higher values of the standard deviation produce the opposite result, and therefore the structural resolution of the modeled capsid is user-defined.

The global density field is evaluated at the points on a regular three-dimensional grid, with lattice-spacing, a, which determines the coarseness or fineness of the resulting surface mesh. An isosurfacing algorithm (here we used the implementation of the marching cubes algorithm (30) from the Visualization Toolkit (31)) is applied to create a surface triangulation representing a constant density. The density range is from 0 outside the capsid or in the center cavity where no atoms are present, to a maximum density, $\rho_{\max}$, somewhere across the shell thickness where the atoms are located in high numbers. A constant density value (the isovalue) is chosen for the inner and

outer surfaces such that the averaged dimensions match those of the atomic structure. We found that an appropriate isovalue is usually roughly $1/2\rho_{max}$, the value used in previous work (32) for reconstruction of low-resolution data from the crystal structure of actin. In this way, we have generated low-resolution density maps and triangulated isosurface meshes from the atomic coordinates of both the native and swollen forms of the CCMV capsid obtained from the Viper Data Bank (29).

Surface mesh construction is illustrated using native CCMV, shown in Fig. 1 *a*. Shown in the figure is a two-dimensional slice of the grid, which has 45 grid points per edge, or a grid spacing of 8 Å. The grid points are color-coded by the value of the global density function calculated at that point. The density values range from 0 to 231. The two black lines represent curves of constant density (density value chosen is 120) in the two-dimensional slice, where linear interpolation is used to determine the exact intersection points. Due to the empty central cavity within the capsid, the single constant density value produces two closed contours, and in three dimensions, the procedure produces two closed triangulated surfaces. The atomic structure of the native CCMV is overlaid onto the final surface triangulation (Fig. 1 *b*). Notably, while a few atoms lie outside of the surface, the contours of the overall structure of CCMV are captured quite well.

Using the triangulated isosurface meshes as input, a tetrahedral volume mesher (here we use the commercial finite element software ABAQUS/CAE (33) for tetrahedral volume meshing) is employed to create three-dimensional tetrahedral meshes discretizing the region between the inner and outer surfaces. Final tetrahedral meshes of the native and swollen CCMV capsids are shown in Fig. 2.

All geometric and mesh parameters are given in Table 1. The grid spacing and value of the standard deviation are chosen to produce a mesh of the coarse-grained representation of the structure with ~10 times fewer vertices than atoms. In practice, the values of the grid spacing and the standard deviation cannot be strictly independent: A lower value of grid spacing is necessary for small standard deviations, to avoid under-resolving the details in the surface. Similarly, a higher value of grid spacing is appropriate for larger standard deviations, to avoid unnecessary fineness of the mesh.

It is not clear a priori how dependent the simulated force-indentation response is on the user-defined levels of structural resolution and mesh resolution. A thorough parametric study of the model, presented elsewhere (M. Gibbons and W. Klug, unpublished), has shown that within a reasonable range of σ-values, the level of structural detail has essentially no effect on the global force-deformation response. The rather coarse models presented in this work (Fig. 2) are within this range.

The density value determining the inner and outer surfaces of the swollen CCMV is selected such that the volume occupied by the tetrahedral meshes of the native and swollen CCMV capsids is the same, consistent with conservation of mass before and after the swelling transition. The number of degrees of freedom for both the native and swollen CCMV meshes are nearly an order-of-magnitude lower than the total number of atoms; a significant reduction that easily allows for the mechanics of large deformation to be simulated for the structure.

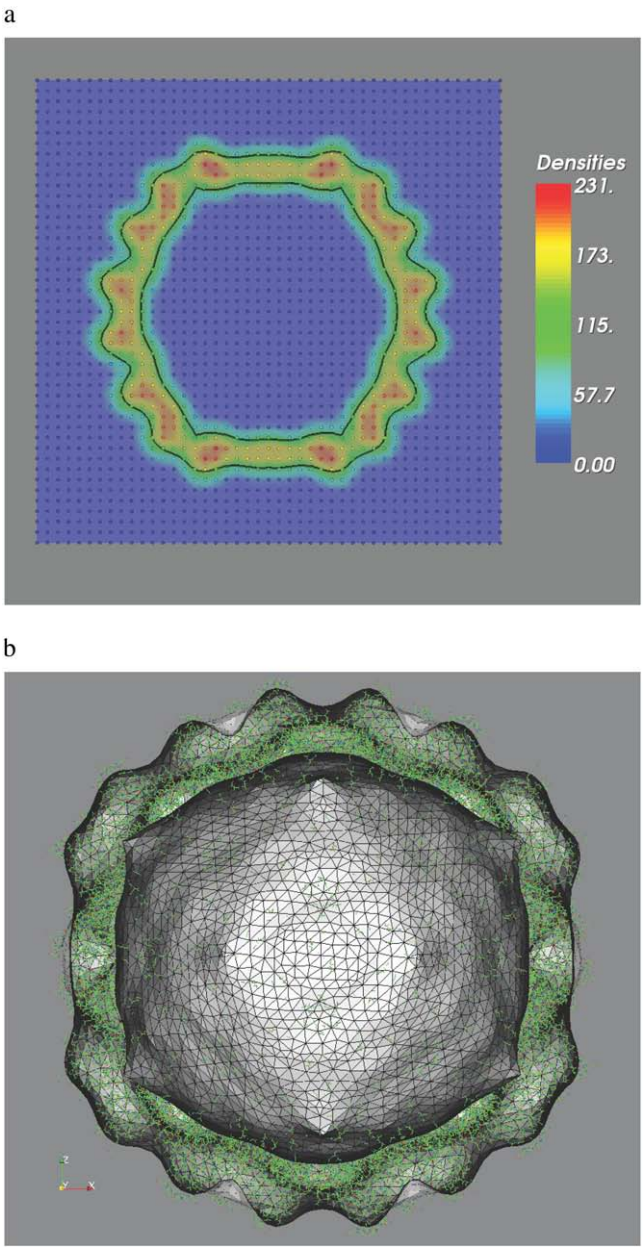

FIGURE 1 (*a*) Two-dimensional slice of a grid showing the scalar density values and the constant density lines cutting through the grid, with a value of 120. (*b*) A cut view of the atomic structure of the native CCMV capsid overlaid onto the three-dimensional surface triangulation created with this method.

Nanoindentation simulations

The capsids are modeled in the framework of finite-deformation continuum hyperelasticity, such that the nonlinear effects of large displacements, rotations, and strains are considered. Using the standard definitions of finite-deformation continuum mechanics (34,35), the deformation of a body is described by the one-to-one deformation mapping $\boldsymbol{\phi}: \beta_0 \rightarrow \mathbb{R}^3$, which maps material point at position $\boldsymbol{X} \in \beta_0$ in the reference configuration of the body to point $\mathbf{x} = \boldsymbol{\varphi}(\boldsymbol{X})$ in the deformed configuration of the body. The deformation gradient tensor is denoted as $\mathbf{F} = \nabla\boldsymbol{\varphi}$, the right Cauchy-Green deformation tensor is denoted as $\mathbf{C} = \mathbf{F}^{\mathrm{T}}\mathbf{F}$, and the volume change ratio of current to reference volume is given by the determinant of the deformation gradient, $J = dv/dV = \det \mathbf{F}$. Hyperelastic material models that specify a strain energy density function, $W(\mathbf{C})$, giving the stored elastic energy per unit reference volume at every material point in the body, and are invariant upon superposed rigid rotations, generally make them the most appropriate choice for large-deformation problems (34,35). Here we use the neo-Hookean model extended to the compressible range, the simplest example of a hyperelastic material with a response that is linear in the first invariant, $I_1 = tr\ \mathbf{C}$,

$$W(\mathbf{C}) = \frac{\mu_0}{2}(I_1 - 3) + \frac{1}{2}\lambda_0(\log J)^2 - \mu_0 \log J, \qquad (2)$$

where the linearized Lamé coefficients λ_0 and μ_0 are related to the Young's modulus E and Poisson's ratio ν as $\lambda_0 = E\nu/[(1 - 2\nu)(1 + \nu)]$ and $\mu_0 = E/2(1 + \nu)$. The stress response is obtained from derivatives of the strain energy density: first Piola-Kirchhoff stress tensor, $\mathbf{P} = \partial W/\partial \mathbf{F}$, or the second Piola-Kirchhoff stress tensor, $\mathbf{S} = 2\partial W/\partial \mathbf{C}$. These stress tensors are related to the Cauchy stress tensor $\boldsymbol{\sigma}$ as $\mathbf{P} = J\boldsymbol{\sigma}\mathbf{F}^{-\mathrm{T}}$, and $\mathbf{S} = J\mathbf{F}^{-1}\boldsymbol{\sigma}\mathbf{F}^{-\mathrm{T}}$. In a

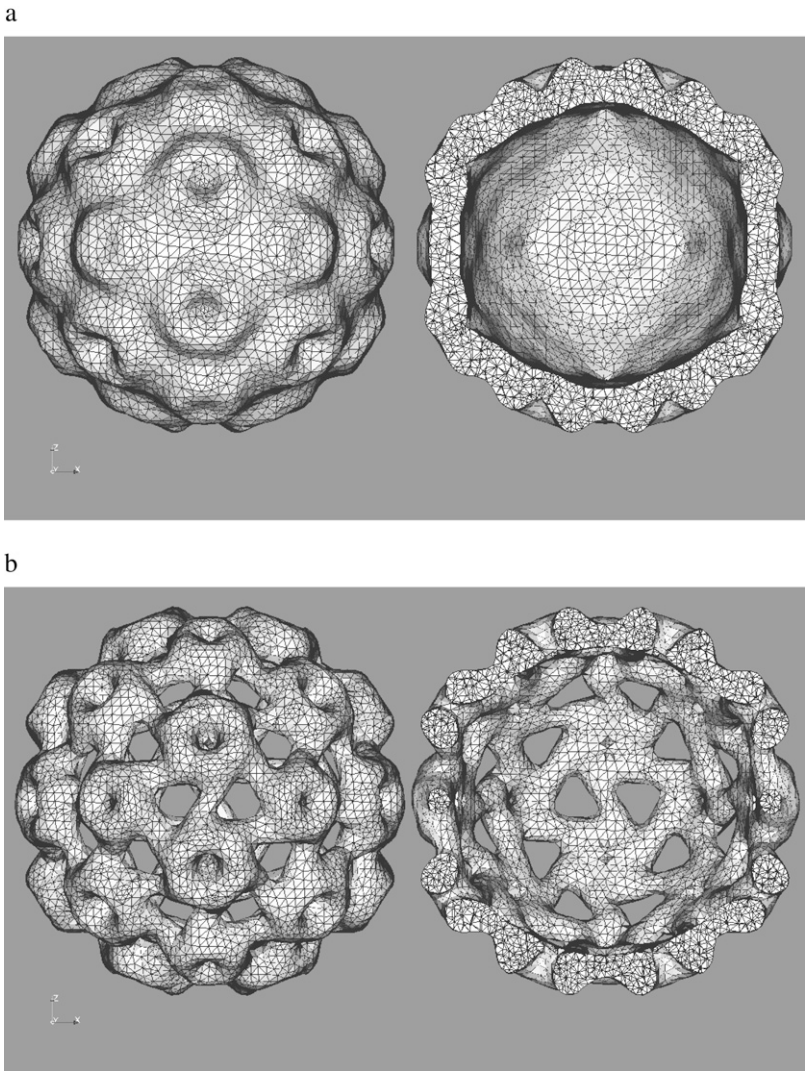

FIGURE 2 Outer and cut views of the (*a*) native and (*b*) swollen CCMV meshes.

previous finite element study in which CCMV was modeled as a spherical shell of uniform thickness (17), we showed that other higher-order forms of the strain energy density function had no appreciable effect on the global force-indentation response. Therefore, we avoid an exhaustive parametric study of constitutive models in this work.

The model of the simulated AFM setup is shown with the glass substrate below and AFM tip above the meshed capsid in Fig. 3. The AFM tip is modeled as a rigid hemisphere with a radius of 20 nm, and the substrate is modeled as a rigid flat plate. Contact between the rigid surfaces and the capsid is modeled as rough friction, wherein points of contact are not allowed to slide tangentially, consistent with the presence of weak adhesion sufficient to keep capsids from sliding out from under the AFM along the surface during the experiments (8,9). Displacement-controlled indentation was simulated on both the native and swollen forms of the CCMV capsid. In each simulation, the total indentation is broken up into 100 equal increments. For the native CCMV, the final indented height at the end of the simulations was set to be 14 nm, with an increment size of 0.13 nm. For the swollen CCMV, the final indented height was set to be 16 nm, with an increment size of 0.16 nm. To assess the effect of orientation on indentation response, separate simulations for both native and swollen capsids were performed with the indentation axis aligned with the twofold (see Fig. 3), threefold, and fivefold symmetry axes.

TABLE 1 Data on atomic structure and tetrahedral meshes for the native and swollen CCMV capsids

	Atomic structure						Finite element mesh	
Capsid	Atoms	d_{avg}	d_{min}	d_{max}	a	σ	Nodes	Elements
Native	214,440	264	201	292	8.1	12	25,946	129,016
Swollen	214,440	305	230	336	7.7	12	32,049	144,081

Note that the atomic structure does not contain hydrogen atoms. Diameters, d; lattice-spacing, a; and density distribution width, σ, are given in Å.

Experimentally, the stiffness of the capsid is given as a spring constant, measured in N/m, which is calculated from the linear portion of the force curve. For the (empty, wild-type) native capsid at pH 5, the spring constant was measured to be ~0.15 N/m (8). To match the experimental spring constant value, the Young's modulus of the model was tuned for the native CCMV capsid, with a value $E = 215$ MPa giving the best agreement (comparable to the previous value of 280 MPa using a spherical shell model (17)). This value is reasonable and consistent with the previously estimated values. The same Young's modulus was also used for the swollen CCMV capsid. As noted above, previous models have suggested that the Young's modulus of CCMV changes with pH (9), thus equivalent values of Young's modulus for the native and swollen forms of the CCMV are likely not physically meaningful. However, using equivalent values for the Young's modulus allows for the isolation of geometric effects on softening. The possibility of combined material and geometric softening is discussed in more detail later. In all cases, a Poisson's ratio of 0.4 was used.

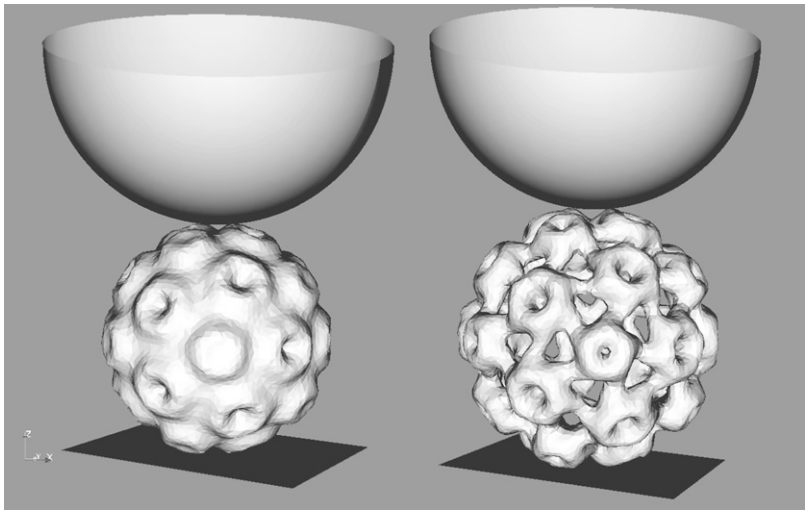

FIGURE 3 Outer views of the modeled experimental setup for the native (*left*) and swollen (*right*) CCMV capsid. Capsids are oriented such that indentation is along a twofold symmetry axis; other orientations not shown. The AFM tip is modeled as a rigid hemisphere with a radius of 20 nm, and the substrate is modeled as a flat, rigid plate.

RESULTS

The force curves produced by simulating indentation along the three icosahedral symmetry orientations of the native CCMV capsid are shown in Fig. 4 *a*. Up to an indentation of ~4 nm, the three curves are nearly coincident and very close to linear, which is consistent with the initial small-strain response. There are two nonlinear features in all three curves that are observed later in the indentation: stiffening, as indicated by a positive curvature; and softening, as indicated by a negative curvature. Stiffening events correspond to discrete changes in contact geometry as additional capsomers contact the AFM tip. As illustrated later in Fig. 6 *a*, the contact area of the twofold orientation is initially confined to two adjacent hexamers, while later additional contact is made with the two nearest pentamers. The point at which the contact area between the capsid and the AFM tip increases is consistent with the stiffening event observed at ~4 nm indentation on the twofold orientation. A similar abrupt increase in contact area between the bottom of the capsid and the substrate also occurs, but slightly earlier in the indentation. (Curvature of the tip away from adjacent capsomers delays contact further than the flat substrate.) However, the increase in stiffness seen in the force-indentation curve occurs only after both the upper and lower portions of the capsid have experienced the increase in contact area, thus the stiffening events appear to be controlled by contact with the AFM tip.

Softening begins only after the shell geometry has become relatively flat underneath the tip, in contrast to the initially curved shell geometry, which is most easily seen in a cut view of the von Mises stress (Fig. 5 *a*). At an indentation of 10 nm, the native twofold capsid is several nanometers past the point at which negative curvature appears in the force curve (~7 nm), and indeed, it appears that the curvature of the shell near the point of contact has actually reversed from the initial configuration. The stress is concentrated at the inner and outer surfaces of the capsid, with the highest stress (outside of the contact regions) existing where the capsid is thinnest, consistent with bending-dominated deformation. From ~7 nm of indentation onwards, the deformation in the capsid is localized to the bending, or wrapping, of the upper portion of the capsid toward the AFM tip.

Both the changes in contact geometry and the geometry of the current deformed configuration affect the load path, or how the AFM tip force is transmitted through the shell down

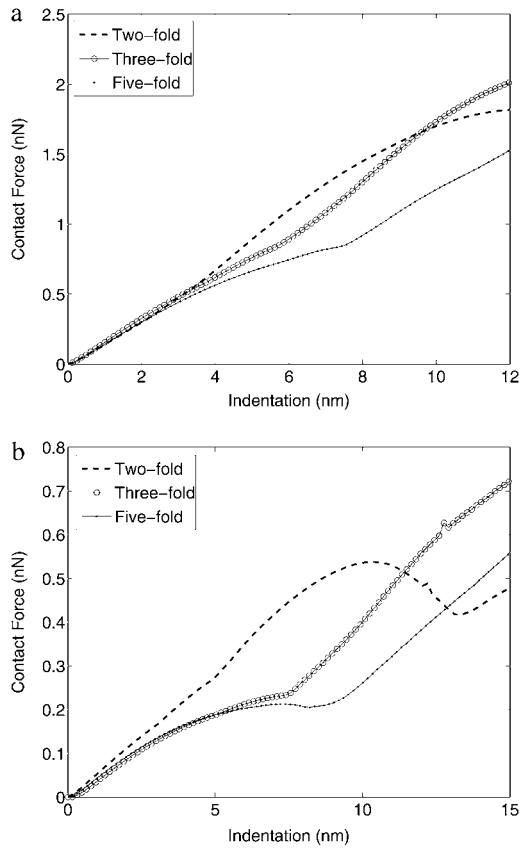

FIGURE 4 Contact force curves for the native (*a*) and swollen (*b*) CCMV indented on each of the rotational symmetry orientations, as a function of the capsid indentation.

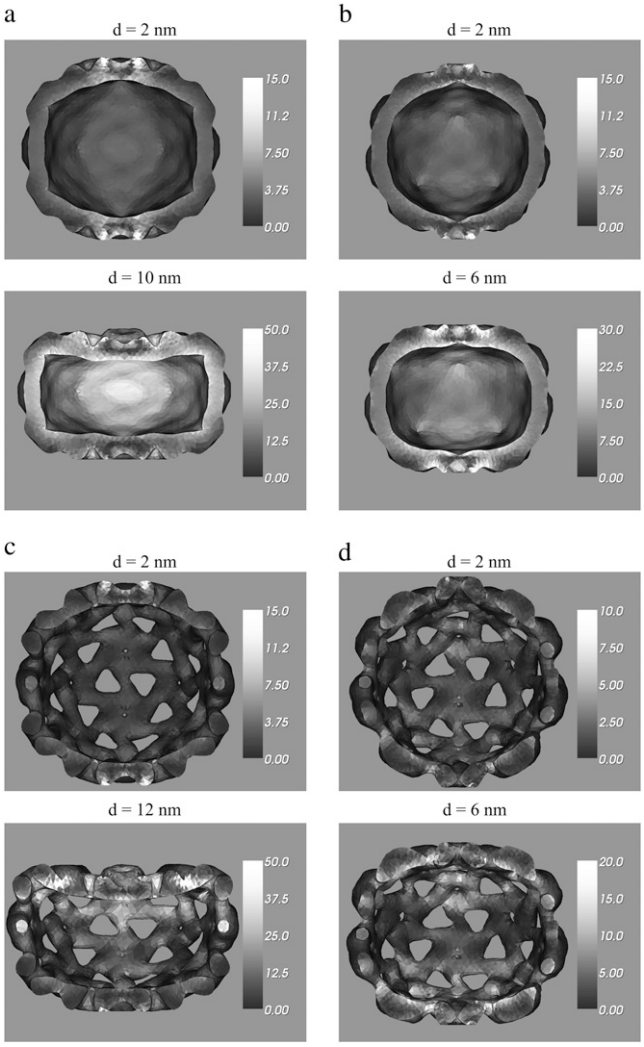

FIGURE 5 Cut side views of the von Mises stress (shown in MPa) at several points during the indentation, illustrating the transition to a bending-dominated motion. This can be seen by viewing the capsomers in the upper portion of the capsids, which undergo very little deformation, but undergo a noticeable rotation.

to the substrate. With increases in the contact area, the indentation forces can be distributed more evenly through the shell, making more efficient use of the material and leading to an overall increased stiffness in the response. The softening events are consistent with a change from stretching-dominated to bending-dominated deformation, as they occur when the shell becomes locally flat such that pure bending is possible. It is a well-known structural mechanics result that bending of a curved shell is always accompanied by stretching, resulting in a response that is stiffer than the bending response of a flat plate (36). Indeed stretch-bending coupling is the primary mechanism that makes curved thin shell structures so efficient at supporting loads (37).

The stiffening and softening behaviors described for the native capsid indented on the twofold symmetry orientation are also present in the curves for the three- and fivefold symmetry orientation curves, although the order of occurrence is reversed. Softening follows the initial linear region, and is then followed by the stiffening events. Changes in contact geometry that cause stiffening are seen on the three- and fivefold symmetry orientations at later points in the indentation, at 6 nm and 8 nm of indentation, respectively. In both cases, the initial contact area is confined to a single hexamer (threefold) or pentamer (fivefold), and the contact area abruptly increases to include the surrounding six and five capsomers, respectively, as seen in Fig. 6 *a*. Softening events consistent with a transition from stretching to bending-dominated deformation occur soon after the initial linear region of 4 nm indentation, with further softening impeded by the sudden increase in contact area described above. Specifically, the areas surrounding the indented hexamer of the threefold and the pentamer of the fivefold orientations have a much lower thickness than the capsomers themselves, and much of the deformation is localized to the bending of this region. The bending response of the fivefold orientation is evident in the cut view of the von Mises stress in Fig. 5 *b*, which shows the nearly flat nature of the shell near the point of contact with the AFM tip at 6 nm of indentation and the concentration of the stresses near the outer edges of the capsid. As in the twofold orientation described above, the highest stresses in the capsid (outside of the contact regions) are in the thin regions between capsomers. The stress response for the capsid indented on the threefold orientation is not shown, as the results are qualitatively similar to that of the fivefold orientation.

Qualitatively, the contact force behavior during indentation on the swollen CCMV capsid is similar to indentation on the native CCMV capsid; the response of the capsid indented on the twofold orientation is generally stiffer, while the responses of the three- and fivefold orientations show more pronounced softening after the initial linear response (see Fig. 4 *b*). Quantitatively, the native and swollen results are quite different. The region of approximately linear response extends only to ~3 nm of capsid indentation, and the response of the capsid indented on the twofold orientation is noticeably stiffer than the other two symmetry orientations, which show dramatic softening. After the initial linear response, the three curves separate noticeably; as in the native case, the nonlinear behavior can be attributed to changes in the local contact geometry (stiffening events) and the transition to bending-dominated deformation (softening behavior). The bending response is amplified in the swollen capsid due to the presence of the holes, which cause a reduction of the effective thickness of the capsid. Additionally, the bending response is much more clearly located in the thin connections between capsomers, with very little, if any, deformation of the capsomers themselves. There is a buckling event that occurs at ~10 nm of indentation on the twofold symmetry orientation, wherein the entire upper area of the capsid bends around the curved surface of the AFM tip. The presence of the holes in the swollen capsid cause the capsomers to be connected with thin bridgelike arms,

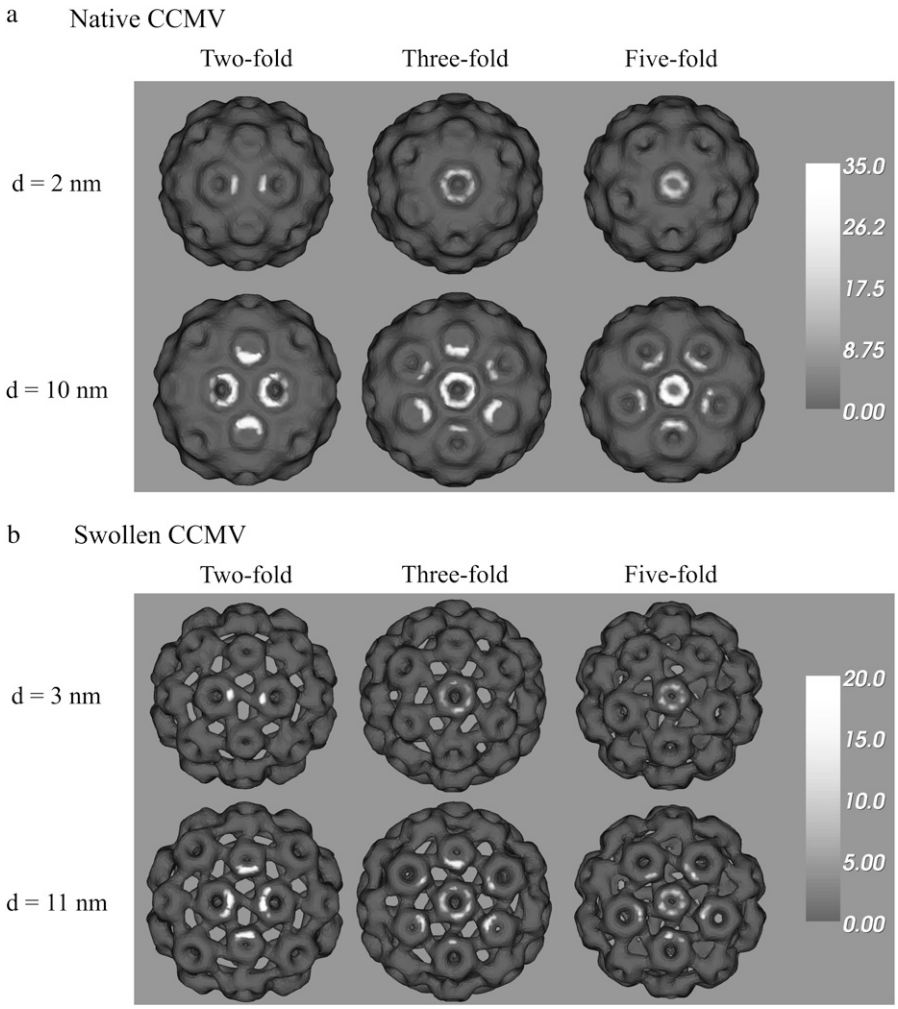

FIGURE 6 Top views of the contact area (showing the magnitude of the nodal contact force, in pN) for (*a*) the native and (*b*) swollen CCMV capsids at several points during the indentation.

and these arms are easily deformed during the buckling event. The sharp upturn in the force curve can again be related to a sudden increase in contact area after the capsid has bent around the AFM tip. The force curves for the three- and fivefold symmetry orientations show marked softening before the sharp upturn, and it is arguable that those orientations are in the process of buckling, but the buckling event is halted by the increase in contact area with the AFM tip that occurs earlier in the indentation than for the capsid in the twofold orientation.

DISCUSSION

The experimental indentation depth on the native CCMV capsid reaches only ~4–5 nm before failure occurs, as evidenced by a steep drop in the force and a drop in the capsid stiffness (8,9). Given that the simulated response at these indentations remains linear—consistent with small-strain shell theory—it is understandable that the experimental force curves are indistinguishable. Due to the failure of the native CCMV capsid observed in experiments, large elastic indentations at which the model predicts geometry-related nonlinearity are physically inaccessible. Furthermore, when the simulated results are plotted as a function of the total displacement of the capsid plus AFM (Fig. 7 *a*), the nonlinearities are almost completely masked, due to the linear response of the AFM cantilever. In this plot, the AFM cantilever is modeled as linearly elastic with spring constant $k = 0.05$ N/m, as reported in Michel et al. (8). To understand the masking of nonlinearity, a straightforward calculation for a linear spring of stiffness k_{afm} in series with a nonlinear spring of stiffness k_{cap} reveals that the curvature c_{tot} of the force versus total displacement response is related to the curvature c_{cap} of the nonlinear spring force response by

$$c_{\text{tot}} = \left(\frac{k_{\text{cap}}}{k_{\text{afm}}} + 1\right)^{-3} c_{\text{cap}}.$$

For the experiments in Michel et al. (8), $k_{\text{cap}}/k_{\text{afm}} \approx 3$, which gives $c_{\text{tot}} \approx c_{\text{cap}}/64$, indicating substantial suppression of nonlinearity in the force response plotted against total displacement. According to this simple calculation, a stiffer cantilever would more accurately represent the nonlinearity of the capsid response; however, stiffening the cantilever can

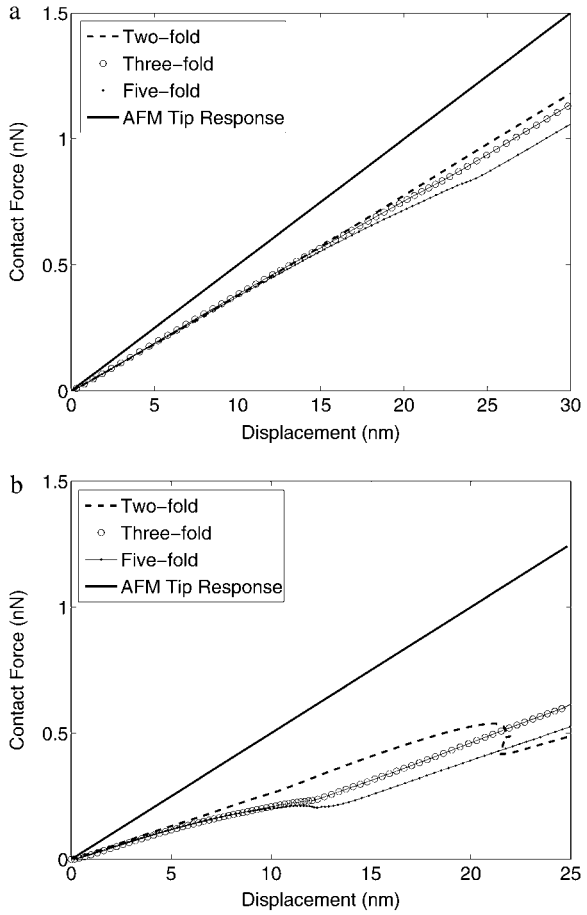

FIGURE 7 Contact force curves for the native (*a*) and swollen (*b*) CCMV indented on each of the rotational symmetry orientations, as a function of the total displacement, which includes the AFM tip displacement (AFM tip $k =$ 0.05 N/m).

decrease the signal/noise ratio of the tip deflection measurement, leading to overall less accurate measurement of the capsid response (38). In principle, the deconvolution operation of subtracting the AFM displacement from the experimental curves is possible, which would allow for direct comparison with the simulated curves of the type shown in Fig. 4. In practice, this deconvolution also decreases the signal/noise ratio, making it difficult to quantify nonlinearity (38). Although these observations are probably not applicable to the native CCMV capsid, as failure occurs before the predicted onset of significant nonlinearity, they might hold some relevance in the interpretation of indentation results of other viruses; in particular, the swollen CCMV capsid and viruses that exhibit nonlinearities at lower indentation values.

To gain clearer perspective on comparing the swollen model to previous experiments, the three contact force curves for the swollen CCMV capsid are plotted versus the total displacement in Fig. 7 *b*. The curves show noticeable softening, roughly by a factor of two relative to those of the native capsid. It is useful to observe that this softening is greater than would be predicted for swelling of a uniformly thick spherical shell. The stiffness of such a shell scales as $k \sim Et^2/R$, where E is the Young's modulus, t the shell thickness, and R the shell radius. Assuming that volume of the shell, scaling as R^2t, is conserved during swelling, a 10% increase of the radius, $R = 1.1\ R_0$, gives $t^2/R = 1.1^{-5}\ t_0^2/R_0$ or $k = 1.1^{-5}\ k_0 \approx 0.62\ k_0$. Hence the factor 0.5 between the stiffnesses of the swollen and native shells in the present geometrically nonuniform models represents even greater significant geometric softening, presumably due to the development of pores and the severe thinning of the ''arm'' regions connecting capsomers in the swollen structure.

In comparison to the geometric softening evident in the present simulations, the experiments presented in Klug et al. (9) observed a stiffness reduction by a factor of three between the native pH 5 and intermediate pH 6 capsid. As previously noted, AFM measurement of height profiles indicate that the pH 6 capsid is not swollen relative to the pH 5 capsid. As there are no detectable structural changes, this seems to rule out the possibility of any geometric softening in the pH 6 case, pointing to pH-triggered changes in protein-protein interactions. It seems likely that the softening from pH 5 to pH 6 is linked to the local changes in the bonding environment (changes or interruptions in the protein-protein interactions at the quasi-threefold orientation) that act to weaken the capsid as a whole, perhaps as a precursor to the actual physical opening of the pores. Since within the continuum elasticity framework, shell stiffness scales linearly with Young's modulus, the pH 5–6 softening can be modeled as a factor-of-three decrease in the effective Young's modulus of the shell.

In the study of Michel et al. (8), the full (packaged) salt-stable mutant was indented by AFM under low pH conditions, and it was found that the stiffness was 50% higher than that of the full wild-type capsid, due to a large number of new protein-protein interactions caused by the point mutation. If this mutant were subjected to experimental AFM indentation while empty at both low and high pH (i.e., in native and swollen forms), which seems feasible given the stable nature of the capsid, the results of the present model suggest that its response would exhibit geometric softening, with the stiffness reduced by a factor of two. Furthermore, based on the pH sensitivity of wild-type CCMV demonstrated in Klug et al. (9), it is conceivable that the salt-stable mutant may also exhibit material softening, which could be by a factor of three or more. However, the effect of the point mutation on pH sensitivity of mechanical properties remains unclear. The precise amount of any further material softening between the pH 6 and pH 7 states cannot be predicted by the current model in the absence of further experimental characterization. AFM indentation experiments would need to be performed to determine the total stiffness change triggered by swelling, from which this model could provide a method to extract the portion attributable to material softening as any additional factor of softness that is measured beyond the factor of two due to geometric softening.

It is possible that, like the native wild-type CCMV capsid, the swollen salt-stable capsid may exhibit material failure before the interesting nonlinear behaviors predicted in this article can be observed, especially given that the holes in the capsid cause the bulk of the forces to be transmitted through the thinnest regions of the capsid, the ''arms'' that connect the capsomers to one another. However, the wild-type capsid exhibited two important features in the transition between pH 5 and pH 6 states: material softening, which has been discussed, and an apparent transition from a brittle to ductile structure that showed no signs of failure. Therefore, it remains a distinct possibility that the fully swollen capsid will inherit the ductile behavior of the pH 6 capsid, and will not fail before observable nonlinear behaviors emerge.

An interesting result of the experiments performed on the native capsid is that although differences in the height profiles were sufficient to determine which symmetry orientation was being indented, the corresponding force curves were indistinguishable (8). This is perhaps surprising, given the difference in local geometry of contact with the AFM tip among the three orientations. This raises the question of whether orientation-dependence of the force response could be enhanced by indentation with different tip sizes. The radius of the AFM tip was varied as a parameter in the previous geometrically simplified three-dimensional models of the native CCMV capsid (17). It was found that by varying the radius of the AFM tip from small (approaching a point load) to infinite (a flat plate), the response at small indentations remained identical, while a slight softening and slight stiffening at larger indentations was observed, respectively. However, due to the simplified nature of the geometry, there were no distinct symmetry orientations on which to indent. In this study, the AFM tip was modeled as a hemisphere with a radius of 20 nm, which is the approximate size of the AFM tip used in the experiments, and it was shown that there are subtle differences in the force curves when indenting on the three symmetry axes, although probably not of a high enough magnitude to observe, due to experimental noise. Therefore, we also simulated indention of the current nonuniform models with several smaller AFM tip sizes, to ascertain the extent to which the size of the tip would produce divergence in the three force curves. The AFM tip radius was lowered to 10 nm and 5 nm, and although lowering the tip radius allows for the three force curves to diverge slightly, this occurs after indentations at which failure is expected to occur (see Fig. 8). Although these results do not suggest any promising new directions for experiments, they do seem to highlight the relative unimportance of the size of the AFM tip on the resulting force curves.

Finally we note that the current modeling techniques presented here are limited to assessing the effect of structural changes on mechanical behavior, whereas the opening of the pores in the CCMV capsid are a symptom of a change at the molecular level that might be described by a change in the material properties. This is one of the drawbacks of employing homogeneous material properties in the current model, and a feature that calls for further future study. It seems that to fully model the mechanical behavior of the CCMV capsid (or any capsid) would require a more detailed material model based on the molecular level response to applied forces. Toward this goal, either homogenization or concurrent multiscale simulation approaches would seem to offer future promise.

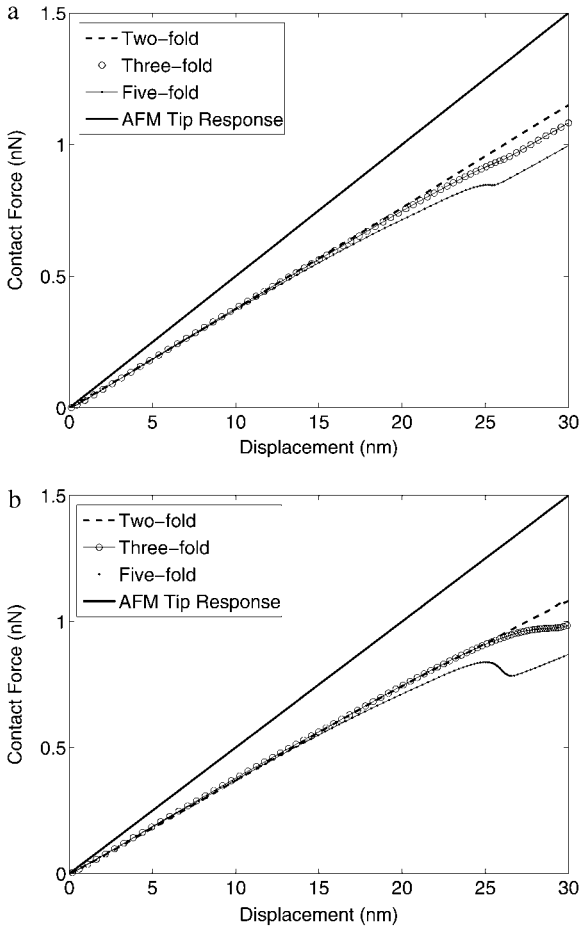

FIGURE 8 Compared contact force curves for the native CCMV mesh indented on each of its rotational symmetry axes, as a function of the total indentation, for an AFM tip with radius (*a*) 10 nm, and (*b*) 5 nm. The curves begin to diverge, but only after indentations at which failure is expected to occur. In both curves, the AFM tip stiffness is set to be $k = 0.05$ N/m.

We thank Charles Knobler, Gijs Wuite, Christoph Schmidt, and Rob Phillips for many insightful discussions, and the reviewers for their insightful comments that helped us to improve the quality of this manuscript.

M.M.G. is supported by a GAANN Fellowship from the U.S. Department of Education.

REFERENCES

1. Douglas, T., and M. Young. 1998. Host-guest encapsulation of materials by assembled virus protein cages. *Nature*. 393:152–155.
2. Douglas, T., E. Strable, D. Willits, A. Aitouchen, M. Libera, and M. Young. 2002. Protein engineering of a viral cage for constrained nanomaterials synthesis. *Adv. Matl*. 14:415–418.
3. Lee, S., C. Mao, C. Flynn, and A. Belcher. 2002. Ordering of quantum dots using genetically engineered viruses. *Science*. 296:892–895.

4. Blum, A., C. Soto, C. Wilson, J. Cole, M. Kim, B. Gnade, A. Chatterji, W. Ochoa, T. Lin, J. Johnson, and B. Ratna. 2004. Cowpea mosaic virus as a scaffold for 3-D patterning of gold nanoparticles. *Nano Lett.* 4:867–870.
5. Kol, N., Y. Shi, M. Tsvitov, D. Barlam, R. Shneck, M. Kay, and I. Rousso. 2007. A stiffness switch in human immunodeficiency virus. *Biophys. J.* 92:1777–1783.
6. Gibbons, M., and W. Klug. 2007. Mechanical modeling of viral capsids. *J. Math. Sci.* 42:8995–9004.
7. Roos, W., I. Ivanovska, A. Evilevitch, and G. Wuite. 2007. Viral capsids: mechanical characteristics, genome packaging and delivery mechanisms. *Cell. Mol. Life Sci.* 64:1484–1497.
8. Michel, J.-P., I. Ivanovska, M. Gibbons, W. Klug, C. Knobler, C. Schmidt, and G. Wuite. 2006. Nanoindentation studies of full and empty viral capsids and the effects of capsid protein mutations on elasticity and strength. *Proc. Natl. Acad. Sci. USA.* 103:6184–6189.
9. Klug, W., R. Bruinsma, J. Michel, C. Knobler, I. Ivanovska, C. Schmidt, and G. Wuite. 2006. Failure of viral shells. *Phys. Rev. Lett.* 97:228101.
10. Bancroft, J. 1970. The self-assembly of spherical plant viruses. *Adv. Virus Res.* 16:99–134.
11. Caspar, D., and A. Klug. 1962. Physical principles in the construction of regular viruses. *Cold Spring Harb. Symp. Quant. Biol.* 27:1–24.
12. Bancroft, J., and E. Hiebert. 1967. Formation of an infectious nucleoprotein from protein and nucleic acid isolated from a small spherical virus. *Virology.* 32:354–356.
13. Speir, J., S. Munshi, G. Wang, T. Baker, and J. Johnson. 1995. Structures of the native and swollen forms of cowpea chlorotic mottle virus determined by x-ray crystallography and cryoelectron microscopy. *Structure.* 3:63–78.
14. Johnson, J., and J. Speir. 1997. Quasi-equivalent viruses: a paradigm for protein assemblies. *J. Mol. Biol.* 269:665–675.
15. Fox, J., X. Zhao, J. Speir, and M. Young. 1996. Analysis of a salt stable mutant of cowpea chlorotic mottle virus. *Virology.* 222:115–122.
16. Ivanovska, I., P. de Pablo, B. Ibarra, G. Sgalari, F. MacKintosh, J. Carrascosa, C. Schmidt, and G. Wuite. 2004. Bacteriophage capsids: tough nanoshells with complex elastic properties. *Proc. Natl. Acad. Sci. USA.* 101:6700–6705.
17. Gibbons, M., and W. Klug. 2007. Nonlinear finite-element analysis of nanoindentation of viral capsids. *Phys. Rev. E Stat. Nonlin. Soft Matter Phys.* 75:031901.
18. Kol, N., M. Gladnikoff, D. Barlam, R. Shneck, A. Rein, and I. Rousso. 2006. Mechanical properties of murine leukemia virus particles: effect of maturation. *Biophys. J.* 91:767–774.
19. Carrasco, C., A. Carreira, I. Schaap, P. Serena, J. Gomez-Herrero, M. Mateu, and P. de Pablo. 2006. DNA-mediated anisotropic mechanical reinforcement of a virus. *Proc. Natl. Acad. Sci. USA.* 103:13706–13711.
20. Vliegenthart, G., and G. Gompper. 2006. Mechanical deformation of spherical viruses with icosahedral symmetry. *Biophys. J.* 91:834–841.
21. Lu, M., and J. Ma. 2005. The role of shape in determining molecular motions. *Biophys. J.* 89:2395–2401.
22. Pettersen, E., T. Goddard, C. Huang, G. Couch, D. Greenblatt, E. Meng, and T. Ferrin. 2004. UCSF Chimera—a visualization system for exploratory research and analysis. *J. Comput. Chem.* 25:1605–1612.
23. Humphrey, W., A. Dalke, and K. Schulten. 1996. VMD—visual molecular dynamics. *J. Mol. Graph.* 14:33–38.
24. Zhang, Y., C. Bajaj, and B. Sohn. 2005. 3D finite element meshing from imaging data. *Comput. Methods Appl. Mech. Eng.* 194:5083–5106.
25. Zhang, Y., and C. Bajaj. 2006. Adaptive and quality quadrilateral/hexahedral meshing from volumetric data. *Comput. Methods Appl. Mech. Eng.* 195:942–960.
26. Bathe, M. 2008. A finite element framework for computation of protein normal modes and mechanical response. *Proteins Struct. Funct. Bioinform.* 70:1595–1609.
27. Reference deleted in proof.
28. Berman, H., K. Henrick, and H. Nakamura. 2003. Announcing the worldwide Protein Data Bank. *Nat. Struct. Biol.* 10:980. http://www.pdb.org/.
29. Shepherd, C., I. Borelli, G. Lander, P. Natarajan, V. Siddavanahalli, C. Bajaj, J. Johnson, I. C. L. Brooks, and V. Reddy. 2006. VIPERdb: a relational database for structural virology. *Nucl. Acids Res.* 34:D386–D389. http://viperdb.scripps.edu/index.php.
30. Lorensen, W., and H. Cline. 1987. Marching cubes: a high resolution 3D surface construction algorithm. *Comput. Graph.* 21:163–169.
31. Schroeder, W., K. Martin, and B. Lorensen. 2004. The Visualization Toolkit. Kitware, Inc., Clifton Park, New York. http://www.vtk.org.
32. Wriggers, W., R. Milligan, K. Schulten, and J. McCammon. 1998. Self-organizing neural networks bridge the biomolecular resolution gap. *J. Mol. Biol.* 284:1247–1254.
33. ABAQUS/CAE v. 6.7. 2007. Dessault Systemes Simulia Corp.
34. Gurtin, M. 1981. An Introduction to Continuum Mechanics. Academic Press, New York.
35. Holzapfel, G. 2001. Nonlinear Solid Mechanics: A Continuum Approach for Engineering. Wiley, New York.
36. Landau, L., and E. Lifshitz. 1986. Theory of Elasticity. Pergamon Press, Oxford.
37. Calladine, C. 1998. Theory of Shell Structures. Cambridge University Press, New York.
38. Wuite, G., and I. Ivanovska. Personal communication.